Fabrication and Evaluation of 5 nm Cathodic-Arc Carbon Films for Disk Drive Applications

by

Walton Fong

Submitted in partial satisfaction
of the requirements for the degree of
Master of Science in Mechanical Engineering

Computer Mechanics Laboratory
Department of Mechanical Engineering
University of California, Berkeley 94720

Abstract

An evaluation of cathodic-arc carbon (CAC) films used as protective overcoats on disk drive media is presented. The material properties of these carbon films are studied first as a function of ion energy during deposition and then as a function of film thickness. It is shown that the most diamond-like properties occur at ion energies of 120 eV and that there is a correlation between film thickness and hardness/elastic modulus. Next, the corrosion performance of these cathodic-arc carbon films is determined by a NaCl decoration test and compared to hydrogenated carbon (CH_x) films. The CAC films significantly outperformed the CHx films and provided continuous coverage at a film thickness of 4 nm. Finally, disks were fabricated with 5 nm CAC overcoats and tested against similar CH_x disks in ultra-high vacuum tribochamber drag tests and thermal desorption studies. The CAC overcoat prevented the catalytic decomposition of ZDOL in drag tests with uncoated sliders. A mechanism for the observed phenomena is proposed with supporting evidence from thermal desorption tests.

1 Introduction

In recent years, the areal density of hard disk drives has increased rapidly, with some sources projecting a continued annual growth rate of 60% in upcoming years [1]. To accommodate this rapid pace, advancements in media and slider technology need to be made. In the slider arena, one approach to increasing areal density has been to reduce the flying height of slider designs toward pseudo-contact, thereby minimizing the magnetic spacing [2]. Similarly, further reduction of the magnetic spacing is possible through the thinning of the protective carbon overcoat layer [3]. But questions arise as to whether or not the conventionally-sputtered carbon overcoats used in today's media will provide the material properties required for acceptable tribological performance in the ultra-thin regime (5 nm thick films).

Currently, carbon overcoats on commercially available disk drive media are deposited by various sputtering techniques. RF sputtering, DC magnetron sputtering, and reactive sputtering are most commonly used for this application [4]. The incorporation of hydrogen and nitrogen during deposition has led to carbon films with improved tribological performance at the head-disk interface (HDI) and spawned the widespread use of amorphous hydrogenated carbon (a-C:H) and nitrogenated carbon (a-C:N) overcoats [5-9]. More recently, ion-beam and filtered cathodic-arc deposition techniques have been investigated in the fabrication of carbon films [10-14]. The interest in these alternative techniques stems from the fact that both can deposit mono-energetic carbon atoms to the surface at ~100 eV, which is suitable for the formation of sp^3 bonds in the

resulting carbon film [10, 15]. These unhydrogenated, highly sp^3 bonded films are commonly referred to as tetrahedral amorphous carbon (ta-C).

Cathodic-arc or vacuum-arc deposition has been in use since the late 1800s and, in the past forty years, most commonly employed to coat cutting tool surfaces [16, 17]. In the early 1990s, Anders et al. pioneered the use of filtered cathodic-arc deposition for disk drive applications with the incorporation of a 90° bent magnetic filter of the Aksenov type to remove the macroparticles (large micron-sized droplets that solidify during flight) generated at the cathode surface [18]. In other experiments, they also demonstrated the benefits of using a pulsed substrate bias to deposit carbon ions at various ion energies [14]. By varying the energy of the carbon ions, one can easily tune the material properties of the carbon film. At ion energies of ~120 eV, the cathodic-arc carbon (CAC) films had an sp^3 content of 85%, hardness of 60 GPa, elastic modulus of 400 GPa, and a density of 3 g/cm^3 [14, 19]. In addition, films fabricated under these conditions exhibited low friction coefficients and extended wear durability.

Since then others have actively conducted research in this area. Various characterization techniques have been applied to studying the material properties and film structures of CAC films including Raman spectroscopy [20, 21], Electron Energy Loss spectroscopy [22], nano-indentation [19], Rutherford backscattering [23], elastic recoil scattering [23], ellipsometry [23], and Fourier Transform IR Spectroscopy [24], to name a few. Of notable mention is the work done by McKenzie et. al. They reported parallel findings to those in Anders et. al [14] in the material properties of CAC films and extended their

efforts into understanding the film stresses generated during deposition and how they affected the film structure [25-27].

A potential drawback of using the cathodic-arc deposition technique is the intrinsic generation of large residual compressive stresses in thicker carbon films that eventually lead to the delamination of the films from the substrate due to adhesion failure at the interface [4]. Anders et. al [28] reported success in counteracting the generation of these stresses using a multilayer approach, depositing alternating layers of hard and soft carbon while retaining the high hardness and elastic modulus of monolithic films. Another technique for relieving these compressive stresses was adopted by Friedmann et. al [29] in their *ex situ* rapid thermal annealing studies of pulsed-laser deposited carbon films. Also, the use of ion implantation during the initial stages of deposition to create an intermediary "mixed" layer at the substrate/film interface alleviated the poor adhesion dilemma by removing the site of the failure [30, 31].

Overall, there is a large and wealthy repository of information in the literature related to CAC films and their properties. Unfortunately, the bulk of this work encompasses CAC films that ranged in thickness from 20 nm to 0.2 μm, a regime that is not directly applicable for use in the future disk drive industry. As we focus on protective carbon overcoats on the order of 5 to 10 nm, questions arise as to whether or not the bulk properties measured previously remain the same in this ultra-thin regime. We are not as concerned about generating large residual compressive stresses from such thin films, but we still insist on good adhesion between the film and the substrate, good film

homogeneity to protect the magnetic layer from environmental effects, and also superior wear durability for long product life. Hence, in this report, we examine the material properties of ultra-thin 5 nm CAC films specifically for disk drive applications, including hardness, elastic modulus, film density, corrosion resistance, wear durability, and surface chemistry. The experimental methods employed include the use of nano-indentation, NaCl decoration tests, high-precision scales (10^{-7} g), UHV tribochamber drag tests, and thermal desorption.

2 Cathodic-Arc Deposition Technique

We begin by reviewing the general working principle of cathodic-arc deposition before continuing with the specific details of our carbon film depositions. The cathodic-arc deposition method is a plasma discharge that occurs between two electrodes in a vacuum. A trigger creates a spark that initiates a high current, low voltage arc. The arc current is concentrated at tiny, discrete spots on the cathode surface, where the cathode material is converted into a plasma that plumes away from the cathode surface [17]. Macroparticles, liquid droplets that are ejected from the surface and solidify during flight, are also created. Various macroparticle filters are incorporated to remove these unwanted particles and to guide the plasma to the substrate surface where high quality thin films are generated [32]. For deposition of uniform films over a large surface area, magnetic ducts are typically placed between the exit of the filter and the substrate for enhanced plasma expansion. A schematic of this deposition method is shown in Figure 1.

To control the energy of the incident carbon ions, a pulsed substrate bias is applied during deposition. Upon exit from the cathode gun, carbon ions have energies on the order of 20 to 30 eV [14]. As they enter the high voltage sheath encompassing the substrate, the carbon ions are accelerated rapidly to energies of 100 eV and higher depending upon the voltage applied to the substrate. Subsequently, by varying the substrate bias, we can easily control the carbon ion energy during deposition and thereby control the film's material properties.

In this work, all the films were deposited in a chamber located at the Lawrence Berkeley National Laboratory. This deposition system consists of a stainless steel vacuum chamber outfitted with various feedthrough ports for power and water-cooling. A base pressure of 1×10^{-6} Torr is achieved through the use of a CTI-Cryogenics Cryoplex 8LP cryopump that is backed by a Trivac D25BCS mechanical pump. The chamber pressure is monitored with a Granville-Phillips 307 vacuum gauge controller and Electron Technology Inc. Bayard-Alpert type ionization gauge.

The following set-up is used to fabricate the cathodic-arc carbon film samples for our studies. A 99.99% pure graphite rod is used as the cathode material and source of C atoms. A General Radio 1340 pulse generator outputs a 5 ms / 1 Hz square wave that is fed into three devices: (1) a Hewlett-Packard 214A pulse generator operating in gated mode that provides a 2 µs ON / 6 µs OFF square wave signal, (2) a custom arc supply that provides the arc current, and (3) a Hewlett-Packard 5532A electronic counter that tracks the number of pulses during a deposition. The custom arc supply provides a

discharge from two capacitor banks – the first capacitor bank discharges 600 V to create the spark while the second bank discharges 350 V to supply the voltage for the duration of the arc. The average current generated by the arc supply during a 5 ms pulse is 250 A. From the HP 214A, the gated signal is then fed into a Cober 605P high power pulse generator that amplifies the voltage from 100 to 2000 V before reaching the water-cooled substrate holder. Hence, the pulsed substrate bias is generated during deposition. Tektronix 2201 and 2430 digital oscilloscopes are used to monitor the arc and substrate bias signals, while a Pearson transformer is implemented to measure the arc current. A flowchart of the deposition process is shown in Figure 2.

To prevent macroparticles from reaching the substrate during deposition, we use a macroparticle filter. Due to the evolution of these magnetic filters during our work, several different designs are used to direct plasma to the substrate while ejecting the macroparticles. The basic working principle of these magnetic filters in guiding the plasma is the same, however [33]. As current flows through the coils of the filter, a magnetic field is generated. Electrons in the plasma entering the filter spiral along these magnetic field lines because their gyration radius is much smaller than the filter size and their collision frequency is smaller than the gyration frequency. The carbon ions in the plasma are not affected by the magnetic field lines, but they follow the guided electrons towards the exit of the filter to keep the plasma quasineutral.

The first of these filters is an open-walled 90° bent filter, shown in operation in Figure 3. This filter design allows approximately 25% of the plasma entering the filter to be

transmitted to the exit [18]. Because the substrate is not in the line-of-sight of the plasma source, macroparticles generated on the cathode surface travel straight through the open-walls of the filter due to their momentum, while the plasma is guided to the filter's exit. However, due to collisions with the coil, some macroparticles reflect off and land on the substrate.

An improvement on this design is the solid-walled S-duct filter, which is two 90° bent filters in series with a bellows wall. As expected, the plasma transmission efficiency of this filter is poor at 6% (0.25 x 0.25 = 0.0625) [34], but the addition of a bellows wall allows macroparticles to be captured or reflected enough times to prevent their emergence at the filter's exit. This filter design is the first to achieve suitable levels of filtration to accommodate the deposition of carbon films for disk drive applications.

Finally, an open-walled S-duct filter in a smaller form factor (radius and curvature) coupled with a physical barrier at the exit provides the best filtering of macroparticles. By increasing the number of coils in the filter at specific locations and reducing the overall length of the filter, the plasma is focused better and transmission efficiency increases to 12-15% [35]. A picture of this S-duct filter in operation is shown in Figure 4.

At the exit of the filter, the plasma expands freely before impinging on the substrate to form carbon films. However, for 65 mm and larger disk substrates, thickness uniformity of the deposited film over these surface areas is critical so we use a magnetic bucket or

homogenizer to expand the plasma rapidly over a short distance to obtain more uniform coatings.

3 Experimental methods

3.1 Nano-indentation

One of the benefits of the cathodic-arc technique for depositing carbon films is the ease in modifying the material properties of the resulting ta-C films. By varying the pulsed substrate bias during deposition, one changes the energy of the impinging carbon ions, which is a critical parameter in depositing predominantly sp^3-bonded films [15]. Changes in the bonding structure of the cathodic-arc carbon films affect material properties such as hardness, which is a material's resistance to plastic deformation, and elastic modulus [19]. In this investigation, we implement the use of a commercially available Hysitron Triboscope system to determine the hardness and elastic modulus of the cathodic-arc carbon films as a function of substrate bias and film thickness.

The Hysitron system [36] is a portable add-on to commercially available atomic force microscopes (AFM). We use a Digital Instruments Nanoscope III in our laboratory. The Hysitron single axis tester is centered around a capacitative force/displacement transducer that provides high sensitivity, a large dynamic range, and a linear force/displacement output signal. A corner of a cubic diamond tip with a nominal radius of 50 nm is used to indent into the sample surface at loads of 1 μN to 10 mN. The TriboScope 3.0 software is used to specify the loading functions, record load/displacement data during indentation, and calculate hardness and elastic modulus of the films.

We define hardness H as

$$H = \frac{P_{max}}{A} \tag{1}$$

where P_{max} is the peak load during indentation and A is the projected contact area at the peak load. Elastic modulus is determined from the following relation (Sneddon) [37]:

$$S = \left.\frac{dP}{dh}\right|_{P\,max} = 2\sqrt{\frac{A}{\pi}}E_r \tag{2}$$

where S is the contact stiffness or slope of the unloading curve at the maximum load, E_r is the reduced modulus, and h is the penetration depth. The reduced modulus is related to the elastic modulus E of the material by

$$\frac{1}{E_r} = \frac{1-\nu^2}{E} + \frac{1-\nu_i^2}{E_i} \tag{3}$$

where ν_i and E_i are the Poisson's ratio and elastic modulus of the indenter, respectively.

The contact area A is a function of contact depth h_c during indentation (i.e. $A=A(h_c)$) and may be found experimentally for a given indenter shape. With this information, the method in Lo and Bogy [36] is used for analyzing the load/unload curve to determine the contact stiffness and subsequently the elastic modulus. Since the possibility of indenter deformation exists with the use of an extremely sharp tip on cathodic-arc carbon films, a correction technique by Lo and Bogy [38] is also incorporated to compensate for this behavior and to calculate true hardness and elastic modulus. Otherwise, an overestimate of the hardness and elastic modulus may occur.

3.1.1 Material properties versus substrate bias

To understand the effects of substrate bias on hardness and elastic modulus, three cathodic-arc carbon films are deposited on low-resistivity, 1" diameter Si <100> wafer substrates. The carbon films are deposited at substrate biases of -100, -500, and –1000 V. We implement the open-walled 90° bent filter for macroparticle reduction and use the following deposition parameters: (1) a base pressure of 1 x 10^{-5} Torr, (2) an arc current of 300A in 5 ms durations at a frequency of 1 Hz, and (3) a pulsed substrate bias with a 33% duty cycle (2 μs ON / 6μs OFF). The first 10% of the deposition is done at a substrate bias of -2000 V for good adhesion between the carbon film and Si wafer. Film thickness is measured with a Dektak IID profilometer. The film thicknesses of the -100, -500, and –1000 V bias samples are 71.5, 122.5, and 98.5 nm, respectively. Hardness and elastic modulus of the CAC films are measured with the Hysitron system. All measurements are limited to indentations with residual depths less than 20% of the total film thickness.

3.1.2 Material properties versus film thickness

To understand the effects of film thickness on hardness and elastic modulus, eight cathodic-arc carbon films are deposited on low-resistivity, 1" diameter Si <100> wafer substrates with film thicknesses ranging from 6.6 to 66 nm. We implement the open-walled 90° bent filter for macroparticle reduction and use the following deposition parameters: (1) a base pressure of 1 x 10^{-5} Torr, (2) an arc current of 300A in 5 ms durations at a frequency of 1 Hz, and (3) a pulsed substrate bias of –100 V with a 33% duty cycle (2 μs ON / 6μs OFF). The first 10% of the deposition is done at a substrate bias of -2000 V for good adhesion between the carbon film and Si wafer. Film

thicknesses are measured with an n & k Analyzer 1100 reflectance spectrometer and Dektak IID profilometer. The film thicknesses of the eight films are 6.6, 10.4, 17.7, 18.2, 23.5, 44, 49, and 66 nm. Hardness and elastic modulus of the CAC films are measured with the Hysitron system. As before, all measurements are limited to indentations with residual depths less than 20% of the total film thickness.

3.2 Density measurements

Another material property closely related to the carbon ion energy during deposition is the film density. Pharr et. al [19] indirectly measured the film density with Electron Energy Loss Spectroscopy (EELS) where the mass density is taken from the valence electron density, which in turn is derived from the valence plasmon. In our investigation, film density measurements are made directly with a high-precision scale with 10^{-7} gram accuracy.

The experimental procedure is as follows. The weights of three low-resistivity, 1" diameter Si <100> wafer substrates are measured with the scale prior to deposition. Next, a small circular area is masked off with a Sharpie permanent ink marker. The carbon films are deposited at substrate biases of -100, -500, and –1000 V. We implement the open-walled 90° bent filter for macroparticle reduction and use the following deposition parameters: (1) a base pressure of 1 x 10^{-5} Torr, (2) an arc current of 300A in 5 ms durations at a frequency of 1 Hz, and (3) a pulsed substrate bias with a 33% duty cycle (2 μs ON / 6μs OFF). The first 10% of the deposition is done at a substrate bias of -2000 V for good adhesion between the carbon film and Si wafer. The samples are then

submerged in an ultrasonic bath of acetone for fifteen minutes to remove the ink and any contamination on the film surface. These wafers are then weighed again and a Dektak IID profilometer is used to determine the film thickness. The film thicknesses of the -100, -500, -1000V bias samples are 71.5, 122.5, and 98.5 nm, respectively. Density values are then calculated directly from the weight difference and film volume as determined by the thickness measurement.

3.3 Corrosion tests

One of the shortcomings of sputter-deposited, amorphous carbon films is their low density and subsequent porous film structure [12]. This results in poor corrosion protection of the magnetic layer as overcoats are reduced to thicknesses less than 10 nm. Cathodic-arc carbon films are well suited for this application as their intrinsic density approaches that of diamond [14, 19, 32, 39], but proper precautions are needed to prevent macroparticles from contaminating the film during deposition. As such, the corrosion resistance of cathodic-arc carbon films is studied in a series of samples with film thicknesses ranging from 2 nm to 40 nm.

These films are deposited on low-resistivity, 1" diameter Si <100> wafers that were previously coated with a layer of 100 nm permalloy (80% Ni / 20% Fe). The CAC films are deposited at a base pressure of 1 x 10^{-5} Torr under these conditions: (1) an arc current of 300 A in 5 ms durations at a frequency of 1 Hz, and (2) a pulsed substrate bias of –100 V with a 33% duty cycle (2 μs ON / 6 μs OFF). The first 10% of the deposition is done at a substrate bias of –2000 V for good adhesion between the carbon film and magnetic

layer. To evaluate the effects of macroparticles on corrosion performance, three sets of films are fabricated with these filter designs (and sample preparation, as appropriate):

1. Solid-walled S-duct filter.
2. Open-walled S-duct filter.
3. Open-walled S-duct filter with sputter cleaning of the permalloy surface prior to deposition.

Sputter-deposited CH_x films (30 atomic % H_2) are used as a reference for this study. Film thicknesses are measured with an n & k Analyzer 1100 reflectance spectrometer and Dektak IID profilometer.

The sputter cleaning procedure involves the introduction of argon gas at a flowrate of 29 sccm to achieve a chamber pressure of 100 mTorr. A glow discharge is initiated at 400V and a current of 14 mA, whereby the permalloy surface is sputter-etched for 5 minutes. Upon completion of the cleaning procedure, the chamber is pumped back down to a base pressure of 1 x 10-5 Torr before deposition of the carbon film begins.

The corrosion performance of these films is based on a simple, yet effective decoration technique – a sodium chloride (NaCl) dip test. Samples were immersed for 24 hours in a pre-mixed solution consisting of 0.5 mol NaCl, 0.5 mol $(NH4)H_2PO_4$, 1 gram Liquinox, and 1000 grams of deionized H_2O. Upon removal, the specimen is rinsed in an ultrasonic bath of deionized water for five minutes and dried with a N_2 air gun. Inspection of the

sample surface is done under an Olympus Vanox optical microscope at 100x magnification, where an image analysis system counts the defect density (number of defects per unit area) in a 0.8 x 1 mm^2 area and defect size (percent area occupied by defects). The image analysis system consists of a Sony Hyper HAD CCD camera interfaced to a computer by a frame grabber board and a Media Cybernetics' Image-Pro Plus software package.

3.4 Ultra-high vacuum (UHV) tribochamber tests

As the disk drive industry approaches near-contact and contact recording, the reduced fly height of slider designs results in more intimate contact between the slider and disk surface for prolonged periods of time [2]. In this regime, not only are mechanical interactions between the slider and disk important, but also chemical reactions between the two surfaces and the lubricant layer. As such, much research is being conducted in this area of tribo-chemistry of the head-disk interface (HDI) [40-43]. A useful tool for studying these tribo-chemical phenomena, especially the decomposition of perfluoropolyether (PFPE) lubricant ZDOL in various environments, is the ultra-high vacuum (UHV) tribochamber developed [44].

The UHV tribochamber consists of a disk spindle, a slider actuator, a substrate heater, and a Balzers QMG 420 high-resolution quadrupole mass spectrometer (QMS) in a stainless-steel vacuum chamber. A base pressure of less than 2 x 10^{-8} Torr is achieved through the use of a Balzers TPU 330 turbo-molecular pump that is backed by a Balzers DUO 016B mechanical pump. The chamber pressure is monitored with two Varian

gauges: a 524-2 cold cathode ionization gauge and a UHV-24 Bayard-Alpert type ionization gauge. The disk spindle is driven by a DC motor at rotational speeds of 50 to 64 rpm through a UHV-compatible feedthrough. A slider may be mounted on the slider actuator, which has a strain arm instrumented with semiconductor strain gauges to measure forces in the vertical and horizontal directions, and its XYZ position is controlled via linear stages. A picture of the tribochamber is shown in Figure 5. More specific details of this system are described in an earlier CML report [44].

The QMS provides in-situ detection of the gaseous products generated at the HDI during drag tests and thermal desorption studies. The QMS can monitor simultaneously 15 different atomic mass units (AMUs) ranging from 1 to 500. We simultaneously obtain friction or temperature data from strain gauge transducers or a thermocouple, respectively. Based on earlier work [45], specific AMUs are monitored during drag tests and thermal desorption studies to examine the decomposition mechanisms of ZDOL: 2 (H_2), 12 (C), 19 (F), 20 (HF), 28 (N_2 or CO), 31 (CF), 44 (CO_2), 47 (CFO), 50 (CF_2), 51 (CF_2H), 66 (CF_2O), 69 (CF_3), 100 (C_2F_4), 116 (C_2F_4O), and 119 (C_2F_5).

3.4.1 Drag tests

The following test procedure is used to conduct drag tests in the tribochamber. Initially, the tribochamber is baked out at 423 K at high vacuum for 24 hours. The chamber is then backfilled with Argon gas as the disk and slider samples are mounted inside. Next, the chamber is pumped down to a base pressure of 2×10^{-8} Torr and the channels of the QMS are assigned to the selected AMUs. The background intensities are recorded before the

drag tests are initiated with the following parameters: 0.1 m/s drag speed, a load of 2.5 grams, and a sliding time of 20 minutes. The mass spectrum and friction data is collected every 2 seconds by a computer connected to the QMS via a serial connection.

The disks used in this study are commercially available, 65 mm smooth thin-film disks. Two sets of disks are tested – both sets are identically manufactured up to the magnetic layer, whereupon one set is sputter-deposited with a 50Å amorphous, hydrogenated carbon overcoat (CH_x) and the second is deposited with 50Å of cathodic-arc carbon. The cathodic-arc carbon is deposited at a base pressure of 1×10^{-5} Torr with the solid-walled S-duct filter under the following conditions: (1) an arc current of 300A in 5 ms durations at a frequency of 1 Hz, and (2) a pulsed substrate bias of –100 V with a 33% duty cycle (2 μs ON / 6μs OFF). The first 10% of the deposition is done at a substrate bias of –2000 V for good adhesion between the carbon film and magnetic layer. Both sets of disks are lubricated with ZDOL by a dipping process and subjected to the same post-processing steps. The molecular weight of ZDOL is 2000 AMU and its chemical formula is given below [46]:

$$CH_2OH\text{-}CF_2O\text{-}(CF_2O)_m\text{-}(CF_2CF_2O)_n\text{-}CF_2\text{-}CH_2OH \text{ where } n/m = 2/3$$

Fourier transform infrared spectroscopy (FTIR) measurements indicated lubricant thicknesses of 8.5Å on the disks.

The sliders used in this study are 50% (1.6 mm by 2 mm) negative-pressure Al_2O_3-TiC sliders with and without amorphous diamond-like carbon (DLC) films on their air bearing surfaces (ABS). The carbon-coated sliders are further separated into two groups: (1) 100Å commercially coated DLC sliders and (2) 50Å CAC-coated sliders fabricated in-house. The deposition parameters for the CAC film on the sliders are identical to those described earlier for the disk samples. A picture of the ABS is shown in Figure 6.

3.4.2 Thermal desorption tests

Prior to conducting thermal desorption tests in the UHV tribochamber, the substrate heater is baked at 589 K in high vacuum for 4 hours to remove any residual contaminants on the heater surface after the previous thermal desorption test. A 2 cm x 2 cm square test sample is cut from each disk. Each sample is mounted on the heater where a thermocouple in contact with the heater is used to monitor the temperature during testing. As with the drag tests, the tribochamber is pumped down to a base pressure of 2×10^{-8} Torr and the channels of the QMS are assigned to the selected AMUs described earlier. The sample is heated at a rate of 0.2 K/s from room temperature to 550 K, while the mass spectrum and temperature data is collected every 2 seconds by a computer connected to the QMS via a serial connection.

The test samples used in this study are cut from commercially available, 65 mm smooth thin-film disks. Two sets of disks are tested – each set is identically manufactured up to the magnetic layer, whereupon one set is sputter-deposited with a 105Å amorphous, hydrogenated carbon overcoat (CH_x) and the second is deposited with 105Å of cathodic-

arc carbon. The deposition parameters for the cathodic-arc carbon are described earlier in Section 3.4.1. Both sets of disks are lubricated with ZDOL (MW 2000) by a dipping process and subjected to the same post-processing steps. FTIR measurements indicated lubricant thicknesses of 12Å on the disks.

4 Results and Discussion

4.1 Nano-indentation

Figure 7 is a plot of the hardness versus substrate bias during deposition of cathodic-arc carbon films. Figure 8 is a similar plot of the elastic modulus of these films. From the charts, we note that the highest hardness (68 GPa) and elastic modulus (244 GPa) belongs to the sample deposited at a –100 V bias, which corresponds to an ion energy of ~120 eV. Weiler et. al [47] and Fallon et al. [48] have published similar hardness levels for carbon films deposited with various methods at ion energies of 90 to 140 eV per incident carbon atom. In addition, the hardness of our film approaches the 90 GPa value typically quoted for polycrystalline diamond [49]. As we increase the substrate bias, both hardness and elastic modulus decrease due to increased graphitization (higher sp^2/sp^3 bonding ratio) of the film. Electron Energy Loss Spectroscopy (EELS) is typically used to determine the sp^3 content of carbon films [10] and an analysis by Pharr et. al [19] on similar films demonstrated that CAC films deposited with a –100 V bias have an sp^3 content of 81% while films deposited at –2 kV had a substantially lower value of 39%.

To determine the effects of film thickness on these two material properties, we refer to Figures 9 and 10, plots of hardness and elastic modulus vs. film thickness for a fixed

substrate bias of –100 V. As we decrease the film thickness from 66 to 6.6 nm, the nano-indentation tests clearly show a reduction in both hardness and elastic modulus. Initial review of this data suggests that the substrate is affecting the nano-indentation measurements, i.e. the underlayer contribution to the hardness of the film increases as the film becomes thinner, which is a common explanation for this phenomenon. However, Lo et. al [50] demonstrated the existence of a surface layer for CAC films that is predominantly sp^2 bonded, whereas the bulk of the film is sp^3 bonded. The ratio of this surface layer thickness to the total film thickness increases for thinner films and hence results in lower hardness values in our nano-indentation tests.

The growth mechanism of this surface layer is still under investigation but we present two popular hypotheses here for discussion. Robertson [10, 51] suggests a subplantation or ballistic model whereby incident ions penetrate the surface into an interstitial site causing a local increase in density. At high enough energies, atoms can migrate back to the surface to relax the excess density forming the sp^2 bonded surface layer. The higher localized densities in the bulk of the film result in sp^3 bonded regions. Thus, a dual-layered film is grown with a softer surface layer over a harder bulk layer. The second model is based upon a similar idea but depends on total film thickness. As film thickness increases, the compressive stress also increases in the film, promoting the formation of sp^3 bonds. This was demonstrated by McKenzie et. al [27] in their studies of compressive-stress-induced formation of ta-C films. For thin films, no appreciable amount of stress is generated so the films remain in an sp^2 bonded state. Hence, thicker films are relatively harder than thinner films due to their higher sp^3 content. Both growth

models support our data, but at this time, we cannot determine which model is correct or if a combination of the two is also possible.

4.2 Density measurements

Figure 11 is a plot of film density versus substrate bias during deposition. Similar to the results from the hardness and elastic modulus study, the highest film density (3.0 g/cm^3) is noted at a pulsed substrate bias of –100 V and decreases to 2.4 g/cm^3 as the bias is increased to – 1 kV. For comparison, the densities of graphite and diamond are 2.25 and 3.51 g/cm^3, respectively. This decrease in film density is the result of a reduction in the compressive stresses of the film. Using a simple theory that accounts for stress generation and stress annealing by ion impacts, Davis [52] demonstrated that the compressive stress increases initially with ion energy and then decreases with further increase of ion energy for ta-C films. For CAC films deposited in our system, we know that this peak corresponds to a substrate bias of – 100V based on earlier work by Ager III et. al [20]. With reduced stress, McKenzie et. al's model [27] predicts less sp^3 hybridization in the films and subsequently lower film density. Moreover, our film density measurements confirm those predicted indirectly by several others with EELS [14, 19, 23, 27].

4.3 Corrosion tests

Figure 12 is a plot of corrosion pinhole count versus film thickness for a fixed substrate bias of –100 V during deposition. Higher pinhole counts imply poorer corrosion-resistance of the film. Three sets of data are plotted on the graph corresponding to the various macroparticle filters used during each deposition. Also on the plot is a line

marking the average pinhole count of 100 for a 7 nm RF-sputtered CH_x film (30 atomic %). This CH_x film is chosen as a reference because it is representative of the protective overcoats on disk drive media currently shipping at the time of this report.

The first set of data, represented by circles, corresponds to films deposited with the solid-walled S-duct filter. No significant difference in corrosion performance is noted for film thicknesses between 4 and 40 nm, which indicates a continuous film on the sample surface even at 4 nm. However, below 4 nm, the pinhole count rises an order of magnitude, which coincides with the values for an uncoated sample, indicating a breakdown of the film continuity/coverage. Hence, the corrosion performance of a 4 nm CAC film with this filter is acceptable for use in today's disk media products.

The second set of data, represented by squares on the plot, corresponds to films deposited with the open-walled S-duct filter. In the 2 to 5 nm film thickness regime, we note that the use of this filter significantly improves the corrosion performance of films compared to those deposited by the solid-walled S-duct filter by reducing the amount of macroparticle contamination. Pinhole counts are in the hundreds instead of the thousands, which is a substantial decrease from the counts we would typically expect for an uncoated sample and also for a 4 nm CH_x film.

By sputter-cleaning the sample surface prior to deposition, we hoped to improve upon the performance of the films deposited with the open-walled S-duct filter. The data corresponding to this third set of films is marked with triangles on the plot. Instead, we

observe no changes in the number of pinhole counts for films in the 2 to 5 nm thickness regime. Thus, no benefit in corrosion performance arises from prior cleaning of the sample surface by sputtering, but it insures the cleanliness of the surface and should be practiced as standard operating procedure for these types of studies.

4.4 UHV tribochamber studies

Figure 13 is a plot of the friction coefficient versus drag time for the 5 nm CAC disk tested with three different types of sliders: (1) uncoated, (2) commercially carbon-coated, and (3) CAC-coated. For the uncoated slider case, the maximum friction coefficient is 2.3 before visual wear is observed after 46 s of dragging. With the addition of a carbon-coating to the slider surface, both wear durability and friction performance improves. The maximum friction coefficient before visual wear for the commercially carbon-coated and CAC-coated slider cases are 0.82 and 0.80, respectively. Also, the wear life for each is extended to 72 s and 60 s of dragging before failure of the head-disk interface is observed.

Figure 14 is a similar plot of the friction coefficient versus drag time for the 5 nm CH_x disk tested with the same three types of sliders. Once again, the worst performance is observed with the uncoated slider case, where maximum friction hits 2.7 before failure occurs after 100 s of dragging. For the commercially available carbon-coated and CAC-coated slider cases, their maximum friction coefficients are 0.75 and 0.29 before failure after 870 s and 140 s of dragging, respectively.

A comparison of the wear durability between the CAC and CH_x disks shows that the CH_x disk outperforms the CAC disk in every slider case. These results are surprising because reports of enhanced wear performance with CAC films have been cited by others. Tsui et. al [53] reported superior scratch resistance of CAC films in nano-scratch tests compared to CH_x films with hydrogen contents ranging from 20 to 40 atomic percent. In another related experiment, Anders et. al [39] demonstrated that disks coated with CAC films reduced the amount of slider ABS erosion compared to CH_x films, which would prevent the formation of particles, initiation of tri-body wear, and subsequent failure of the interface. However, in those studies, their films were much thicker than those of interest here, and citing our earlier nano-indentation results, the difference in material properties due to the film thickness effect are significant. These differences may account for the poor performance in our drag tests with the CAC films.

In terms of friction, the use of various different sliders greatly affects the values recorded during the drag test. For both CAC and CH_x disks, the highest coefficient of friction (COF) is observed with the uncoated sliders due to the material incompatibility between the slider (Al_2O_3-TiC) and disk (carbon) surface. Using sliders with a carbon-coating reduces the COF and prolongs the life of the head-disk interface as expected [54, 55]. On the CAC disk, no significant difference in friction performance is noted between the commercially available carbon-coated slider and CAC-coated slider. However, on the CH_x disk, the CAC-coated slider provides a COF half that of the commercially available carbon-coated slider, an observation noted by others in similar experiments [56].

Next, we examine the effects of the carbon overcoat on the decomposition mechanisms of the ZDOL lubricant layer. The decomposition of ZDOL may be broken down into two primary mechanisms, frictional/thermal decomposition and catalytic decomposition. Masses 47 (CFO) and 66 (CF_2O) are recorded to monitor the extent of the frictional or thermal decomposition of ZDOL. A synopsis of the frictional decomposition mechanism is listed below and is based on extensive work by Chen et. al [40, 41, 43], Wei et. al [45], and Yun et. al [44]. Further details of the decomposition may be found in their papers.

$$\text{-O-/-}CF_2\text{-O-/-}CF_2\text{-}CF_2\text{-0-/-}CF_2\text{-} \Rightarrow CF_2{=}O\ (66) + \text{-}CF_2\text{-}CF_2\text{-O-}\ (116) \qquad (4)$$

$$\text{-}CF_2\text{-}CF_2\text{-O-}\ (116) \Rightarrow \text{-}CF_2\text{-}\ (50) + CF_2{=}O\ (66) \qquad (5)$$

$$CF_2{=}O\ (66) \Rightarrow CFO\ (47) + F\ (19) \qquad (6)$$

In this process, the ZDOL molecule decomposes under friction action alone by chemical reactions 4 and 5. The gaseous by-products from these reactions are then further cleaved by electron bombardment in the mass spectrometer as described in reaction 6.

The catalytic decomposition mechanism is much more complex. We monitor masses 69 (CF_3) and 119 (C_2F_5) during the drag tests to determine the extent of this reaction. Once again, this mechanism is based on the work by Chen et. al [40, 41, 43], but important components are also derived from the results of Kasai et. al's [57] chemical studies with ZDOL in the presence of slider material Al_2O_3-TiC. It begins with the by-products generated by frictional stimulation of the interface described in reaction 4. In addition, hydrogen evolves from the interface and reacts to form hydrofluoric acid (HF). The

CF_2=O and HF from these two reactions then interact with the Al_2O_3 from the slider surface to produce Lewis acid AlF_3 as shown in reactions 7 and 8.

$$Al_2O_3 + 6\ HF \Rightarrow AlF_3 + 3\ H_2O \quad (7)$$

$$Al_2O_3 + 3\ CF_2O \Rightarrow 2\ AlF_3 + 3\ CO_2\ (44) \quad (8)$$

Rapid reactions along the main ZDOL chain take place on the AlF_3 surface to form CF_3-O-, CF_3CF_2-O- compounds, and R-CF=O:

$$R\text{-}CF_2\text{-}O\text{-}CF_2\text{-}R \Rightarrow \begin{matrix} F \\ R\text{-}C{=}O \end{matrix} + CF_3\text{-}R \quad (9)$$

(CF_3-R: CF_3-O-, CF_3CF_2-O-)

Subsequent electron impacts in the mass spectrometer lead to CF_3 (69) and CF_3CF_2 (119) fragments.

Figure 15 is a plot of the integrated mass spectrum over the first eighty cycles of dragging on the CH_x disk for four different mass fragments: 47 (CFO), 66 (CF_2O), 69 (CF_3), and 119 (C_2F_5). Three sets of data are plotted in this figure corresponding to the various sliders used during the drag test. First, we observe that the highest intensities are associated with the uncoated slider. Masses 69 and 119 are an order of magnitude higher than that for the carbon-coated slider cases – this is expected as the carbon film on the slider surface acts as a physical barrier between the lubricant and the Al_2O_3-TiC slider material to prevent the catalytic decomposition from occurring. Masses 47 and 66 are

also higher than that for the carbon-coated slider cases and this difference is due to the higher COF we observe during the drag tests, i.e. higher friction results in more shearing/scissioning of the ZDOL molecule. No significant difference is noted between the results for the commercially available carbon-coated slider and CAC-coated slider. Both coatings prevent the catalytic decomposition of ZDOL from occurring.

Figure 16 is a similar plot of the integrated mass spectrum for the CAC disk. We note a slightly more than two-fold decrease in the intensities of masses 69 and 119 compared to those for the CH_x disk, indicating that the use of a CAC overcoat reduces the catalytic decomposition of ZDOL. These results confirm our earlier reports of a two-fold reduction in the catalytic decomposition of ZDOL when using CAC instead of CH_x overcoats on disks in drag tests [42]. Surprisingly, for the carbon-coated slider cases, both sliders exhibit higher intensities in masses 47 and 66 for the CAC disk compared to the CH_x disk. No significant differences in the friction coefficient could account for this increase. Instead, a measurement of the lubricant thickness via FTIR on both disks revealed that the CAC disk had twice as much lubricant as the CH_x disk (1 nm vs. 0.5 nm). Chen et. al [58] reported that the mass fragment intensities measured in these types of studies are highly dependent on lubricant thickness – the intensity scales with lubricant thickness. Thus, we observe consistently higher intensities for all the masses in the carbon-coated slider cases of the CAC disk compared to the CH_x disk. Remarkable, though, is the fact that the CAC disk significantly decreases the catalytic decomposition of ZDOL with uncoated sliders compared to the CH_x disk when we account for this lubricant thickness disparity between the two samples.

To understand why CAC films prevent the catalytic decomposition of ZDOL in drag tests, we turn to the thermal desorption experiments. Figure 17 is the thermal desorption profile for H_2, i.e. the intensity of H_2 as a function of temperature, for both the CAC and CH_x disks. We observe that the amount of hydrogen evolving from the CAC sample (interpreted as the area under the curve) is orders of magnitude lower than that for the CH_x sample. Figures 18 and 19 are similar desorption profiles for fluorine (F) and hydrofluoric acid (HF), respectively. We again note that the CAC sample generates much less F and subsequently less HF than its CH_x counterpart. Hence, the CAC films evolve less H_2 than CH_x films, which hinders the catalytic decomposition mechanism of ZDOL described earlier. We propose that without a source of hydrogen, HF production is limited and prevents the formation of the Lewis acids required for the rapid decomposition of the ZDOL chain. This is a significant result in our understanding of the critical components of the decomposition of ZDOL, as it also reveals the benefit of using CN_x overcoats, which has been discussed in another CML report [41].

5 Conclusions

The use of cathodic-arc carbon (CAC) films as a protective overcoat for disk drive media as an alternative to conventionally sputtered, hydrogenated carbon films (CH_x) is investigated. In this report, we demonstrated that the material properties of CAC films are highly dependent upon ion energy of C atoms during deposition and that the most diamond-like films are observed when this energy is approximately 120 eV. Moreover, these material properties are dependent upon the thickness of the CAC film due to the

inherent formation of a dual-layered film structure with an sp^2-bonded surface layer and an sp^3-bonded bulk layer. At a film thickness of 4 nm, CAC films remained continuous, provided acceptable levels of corrosion resistance by today's disk drive standards, and significantly outperformed CH_x films. 5 nm CAC disks also prevented the catalytic decomposition of ZDOL in UHV drag tests with uncoated sliders by generating less H_2 at the head/disk interface. This reduced hydrogen evolution in turn hindered the formation of hydrofluoric (HF) and Lewis acids (AlF_3) required to decompose the ZDOL molecule. However, the wear performance of CAC disks was not comparable to that of the CH_x disks - due most likely to the highly graphitic nature of the CAC films at 5 nm - but further work in modifying the deposition parameters may provide a solution to this deficiency.

6 Acknowledgments

We extend many thanks to Dr. Simone Anders, Dr. Othon Monteiro, Dr. Andre Anders, and Dr. Ian Brown for the use of their cathodic-arc deposition chamber and providing countless hours of advice and suggestions in this work; Roger Yu Lo for providing the much needed nano-indentation results; Chao-Yuan Chen for his many helpful discussions on lubricant decomposition; and last, but not least, Dr. C. Singh Bhatia for generously supplying the materials, post-test analysis, and his time to finish this project. This research project was supported by the National Storage Industry Consortium and the Computer Mechanics Laboratory at the University of California at Berkeley.

7 References

[1] Waid, D. and Ajk, Toren, "Magnetic Storage: What Does the Future Hold?," *IDEMA Insight*, May/June 1999, pp. 7 and 38.

[2] Hsia, Y. and Donovan, M., "The Design and Tribology of Tripad Sliders for Pseudo-Contact Recording in Magnetic Hard Disk Drives," Tribology of Contact/Near-Contact Recording for Ultra High Density Magnetic Storage (TRIB-Vol.6), Proceedings of 1996 ASME/STLE International Tribology Conference and Exposition, San Francisco, CA, USA, October 13-18, 1996, p.17-23.

[3] Bhusan, B., *Tribology and Mechanics of Magnetic Storage Devices*, Springer, New York, 1990.

[4] Ohring, M., *The Materials Science of Thin Films*, Academic Press, San Diego, 1992.

[5] Cutiongco, E. C., Li, D., Chung, Y., and Bhatia, C. S., "Tribological Behavior of Amorphous Carbon Nitride Overcoats for Magnetic Thin-Film Rigid Disks," *Journal of Tribology*, Vol. 118, July 1996, pp. 543-548.

[6] Agarwal, S. and Li, E., "Structure and Tribological Performance of Carbon Overlayer Films," *IEEE Transactions on Magnetics*, Vol. 29, No. 1, January 1993, pp. 264-269.

[7] Marchon, B., Vo, P. N., and Khan, M. R., "Structure and Mechanical Properties of Hydrogenated Carbon Films Prepared by Magnetron Sputtering," *IEEE Transactions on Magnetics*, Vol. 27, No. 6, November 1991, pp. 5160-5162.

[8] Wang, R., Meeks, S., White, R., and Weresin, W., "The Effect of Hydrogen in Carbon Overcoats on the Tribology of the Head-Disk Interface," *IEEE Transactions on Magnetics*, Vol. 31, No. 6, November 1995, pp. 2919-2921.

[9] White, R., Bhatia, S. S., Meeks, S., Friedenberg, M., and Mate, C. M., "RF-Sputtered Amorphous CNx for Contact Recording Applications," Tribology of Contact/Near-Contact Recording for Ultra High Density Magnetic Storage (TRIB-Vol.6), Proceedings of 1996 ASME/STLE International Tribology Conference and Exposition, San Francisco, CA, USA, October 13-18, 1996, p.33-38.

[10] Robertson, J., "Deposition and Properties of Diamond-Like Carbons," to be published in *Properties and Processing of Vapor-Deposited Coatings*,

Proceedings of 1998 Fall Meeting of Materials Research Society Symposium, Boston, Massachusetts, USA, November 30 - December 2, 1998, Vol. 555.

[11] Weiler, M., Lang, K., Li, E., and Robertson, J., "Deposition of tetrahedral hydrogenated amorphous carbon using a novel electron cyclotron wave resonance reactor," *Applied Physics Letters*, Vol. 72, No. 11, March 1998, pp. 1314-1316.

[12] Robertson, J., "Properties of Diamond-Like Carbon," *Surface and Coatings Technology*, Vol. 50, 1992, pp. 185-203.

[13] Anders, A., "Metal Plasma Immersion Ion Implantation and Deposition: A Review," *Surface and Coatings Technology*, Vol. 93, 1997, pp. 158-167.

[14] Anders, S., Anders, A., Brown, I., Wei, B., Komvopoulos, K., Ager III, J. W., and Yu, K. M., "Effect of Vacuum Arc Deposition Parameters on the Properties of Amorphous Carbon Thin Films," *Surface and Coatings Technology*, Vol. 68/69, 1994, pp. 388-393.

[15] Veerasamy, V. S., Amaratunga, G. A. J., Milne, W. I., Robertson, J., and Fallon, P. J., "Influence of Carbon Ion Energy on Properties of Highly Tetrahedral Diamond-Like Carbon," *Journal of Non-Crystalline Solids*, Vol. 164-166, 1993, pp. 1111-1114.

[16] Sanders, D., Boercker, D., and Falabella, S., "Coating Technology Based on the Vacuum Arc – A Review," *IEEE Transactions on Plasma Science*, Vol. 18, No. 16, December 1990, pp. 883-894.

[17] Brown, I., "Vacuum Arc Ion Sources," *Rev. Sci. Instrum*., Vol. 65, No. 10, October 1994, pp. 3061-3081.

[18] Anders, A., Anders, S., and Brown, I., "Transport of Vacuum Arc Plasmas Through Magnetic Macroparticle Filters," *Plasma Sources Sci. Technology*, Vol. 4, 1995, pp. 1-12.

[19] Pharr, G. M., Callahan, D. L., McAdams, S. D., Tsui, T. Y., Anders, S., Anders, A., Ager , J. W., Brown, I. G., Bhatia, C. S., Silva, S. R. P., and Robertson, J., "Hardness, Elastic Modulus, and Structure of Very Hard Carbon Films Produced by Cathodic-Arc Deposition with Substrate Pulse Biasing," *Appl. Phys. Lett*., Vol. 68, No. 6, February 1996.

[20] Ager III, J. W., Anders, S., Anders, A., and Brown, I., "Effect of Intrinsic Growth Stress on the Raman Spectra of Vacuum-arc-deposited Amorphous Carbon Films," *Applied Physics Letters*, Vol. 66, No. 25, June 1995, pp. 3444-3446.

[21] Tay, B. K., Shi, X., Tan, H. S., Yang, H. S., Sun, Z., "Raman Studies of Tetrahedral Amorphous Carbon Films Deposited by Filtered Cathodic Vacuum Arc," *Surface and Coatings Technology*, Vol. 105, 1998, pp. 155-158.

[22] Davis, C. A., Knowles, K. M., and Amaratunga, G. A. J., "Cross-sectional Structure of Tetrahedral Amorphous Carbon Thin Films," *Surface and Coatings Technology*, Vol. 76-77, 1995, pp. 316-321.

[23] Lossy, R., Pappas, D. L., Roy, R. A., Doyle, J. P., Cuomo, J. J., and Bruley, J., "Properties of Amorphous Diamond Films Prepared by a Filtered Cathodic Arc," *J. Appl. Phys*., Vol. 77, No. 9, May 1995, pp. 4750-4756.

[24] Coll, B. F., Sathrum, P., Aharonov, R., and Tamor, M. A., "Diamond-like Carbon Films Synthesized by Cathodic Arc Evaporation," *Thin Solid Films*, Vol. 209, 1992, pp. 165-173.

[25] McKenzie, D. R., Yin, Y., Marks, N. A., Davis, C. A., Pailthorpe, B. A., Amaratunga, G. A. J., Veerasamy, V. S., "Hydrogen-free Amorphous Carbon Preparation and Properties," *Diamond and Related Materials*, Vol. 3, 1994, pp. 353-360.

[26] McKenzie, D. R., Yin, Y., Marks, N. A., Davis, C. A., Kravtchinskaia, E., Pailthorpe, B. A., Amaratunga, G. A. J., "Tetrahedral Amorphous Carbon Properties and Applications," *Journal of Non-Crystalline Solids*, Vol. 164-166, 1993, pp. 1101-1106.

[27] McKenzie, D. R., Muller, D., and Pailthorpe, B. A., "Compressive-Stress-Induced Formation of Thin-Film Tetrahedral Amorphous Carbon," *Physical Review Letters*, Vol. 67, No. 6, August 1991, pp. 773-776.

[28] Anders, S., Callahan, D. L., Pharr, G. M., Tsui, T. Y., Bhatia, C. S., "Multilayers of Amorphous Carbon Prepared by Cathodic Arc Deposition," *Surfaces and Coating Technology*, Vol. 94-95, No. 1-3, October 1997, pp. 189-194.

[29] Friedmann, T. A., Sullivan, J. P., Knapp, J. A., Tallant, D. R., Follstaedt, D. M., Medlin D. L., and Mirkarimi, P. B., "Thick Stress-Free Amorphous-Tetrahedral Carbon Films with Hardness Near that of Diamond," *Appl. Phys. Lett*., Vol. 71, No. 26, December 1997.

[30] Gerstner, E. G., McKenzie, D. R., Puchert, M. K., Timbrell, P. Y., and Zou, J., "Adherent Carbon Film Deposition by Cathodic Arc with Implantation," *J. Vac. Sci. Technol. A*, Vol. 13, No. 2, March/April 1995, pp. 406-411.

[31] Anders, A., Anders, S., Brown, I., Dickinson, M. R., MacGill, R. A., "Metal Plasma Immersion Ion Implantation and Deposition Using Vacuum Arc Plasma Sources," *J. Vac. Sci. Technol. B*, Vol. 12, No. 2, March/April 1994, pp. 815-820.

[32] Anders, S., Bhatia, C. S., Fong, W., Lo, R., Bogy, D., "Application of Cathodic Arc Deposited Amorphous Hard Carbon Films to the Head/Disk Tribology," to be published in Proceedings of 1998 Spring Meeting of the Materials Research Society, San Francisco, CA, April 13-17, 1998.

[33] Anders, A., "Approaches to Rid Cathodic Arc Plasmas of Macro and Nanoparticles: A Review," to be published in *Surface and Coatings Technology*.

[34] Anders, S., Anders, A., Dickinson, M. R., MacGill, R. A., Brown, I.G., "S-shaped Magnetic Macroparticle Filter for Cathodic Arc Deposition," *IEEE Trans. Plasma Sci*., Vol. 25, August 1997, pp. 670-674.

[35] Anders, A., personal communication, August 30, 1999.

[36] Lo, R. and Bogy, D. B., "On the Measurement of Nano-Hardness and Elastic Modulus of Ultra-Thin Overcoats: Effect of W-doping and Annealing on the Properties of DLC," *Technical Report 97-017 (Blue Series)*, Computer Mechanics Laboratory, University of California, Berkeley, CA, September 1997.

[37] Sneddon, I. N., "The Relation Between Load and Penetration in the Axisymmetric Boussinesq Problem for a Punch of Arbitrary Profile," *Int. J. Eng. Sci*., Vol. 3, 1965, pp. 47-57.

[38] Lo, R. and Bogy, D. B., "Compensating for Indenter Deformation While Indenting on Very Hard Materials," *Technical Report 98-005 (Blue Series)*, Computer Mechanics Laboratory, University of California, Berkeley, CA, June 1998.

[39] Anders, S., Brown, I., and Bogy, D., "Wanted: Hard, Thin Coatings for Near-Contact Recording," *Data Storage*, Vol. 4, No. 9, October 1997, pp. 31-34.

[40] Chen, C. Y., Fong, W., Bogy, D., and Bhatia, C. S., "The Decomposition Mechanisms and Thermal Stability of ZDOL Lubricant on Hydrogenated Carbon Overcoats," *Technical Report 98-016 (Blue Series)*, Computer Mechanics Laboratory, University of California, Berkeley, CA, December 1998.

[41] Chen, C. Y., Fong, W., Bogy, D., and Bhatia, C. S., "Initiation of Lubricant Catalytic Decomposition by Hydrogen Evolution from Contact Sliding on CHx Overcoats," *Technical Report 99-011 (Blue Series)*, Computer Mechanics Laboratory, University of California, Berkeley, CA, August 1999.

[42] Bhatia, C. S., Fong, W., Chen, C. Y., Wei, J., Bogy, D., Anders, S., Stammler, T., and Stohr, J., "Tribo-Chemistry at the Head/Disk Interface," *IEEE Transactions on Magnetics*, Vol. 35, No. 2, March 1999, pp. 910-915.

[43] Chen, C. Y., Fong, W., Bogy, D., Bhatia, C. S., "Tribochemistry of Monodispersed ZDOL with Hydrogenated Carbon Overcoats," *Technical Report 99-008 (Blue Series)*, Computer Mechanics Laboratory, University of California, Berkeley, CA, May 1999.

[44] Yun, X. H. and Bogy, D. B., "Tribochemical Study of Hydrogenated and Nitrogenated Overcoats at the Head Disk Interface in Magnetic Hard Drives," *Doctoral Dissertation 96-002 (Gold Series)*, University of California, Berkeley, CA, June 1996.

[45] Wei, J., Fong, W., Bogy, D. B., and Bhatia, C. S., "The Decomposition Mechanisms of a Perfluoroether at the Head/Disk Interface of Hard Disk Drives," *Tribology Letters*, Vol. 5, No. 2-3, 1998, pp. 203-209.

[46] Product data for Fomblin Z lubricants, Ausimont, undated.

[47] Fallon, P. J., Veerasamy, V. S., Davis, C. A., Robertson, J., Amaratunga, G. A. J., Milne, W. I., and Koskinen, K., "Properties of Filtered-Ion-Beam-Deposited Diamondlike Carbon as a Function of Ion Energy," *Physical Review B*, Vol. 48, 1993, p. 4777.

[48] Weiler, M., Sattel, S., Jung, K., Ehrhardt, H., Veerasamy, V. S., and Robertson, J., "Highly Tetrahedral, Diamond-Like Amorphous Hydrogenated Carbon Prepared from a Plasma Beam Source," *Applied Physics Letters*, Vol. 64, No. 21, May 1994, pp. 2797-2799.

[49] Brookes, C. A., Properties of Diamond, Academic Press, New York, 1979.

[50] Lo, R., Fong, W., Bogy, D. B., and Bhatia, C. S., "Thickness Dependence of Hardness and Elastic Modulus of Cathodic-Arc Amorphous Carbon Films," *Technical Report 98-012 (Blue Series)*, Computer Mechanics Laboratory, University of California, Berkeley, CA, November 1998.

[51] Robertson, J., "Deposition Mechanism of a-C and a-C:H," *Journal of Non-Crystalline Solids*, Vol. 164-166, 1993, pp. 1115-1118.

[52] Davis, C. A., "A Simple Model for the Formation of Compressive Stress in Thin Films by Ion Bombardment," *Thin Solid Films*, Vol. 226, No. 1, April 1993, pp. 30-34.

[53] Tsui, T. Y., Pharr, G. M., Oliver, W. C., Bhatia, C. S., White, R. L., Anders, S., Anders, A., and Brown, I. G., "Nanoindentation and Nanoscratching of Hard Carbon Coatings for Magnetic Disks," Proceedings of 1995 Materials Research Society Mechanical Behavior of Diamond and Other Forms of Carbon Symposium, San Francisco, CA, USA, April 17-21, 1995, p.447-52.

[54] Bogy, D. B., Yun, X., and Knapp, B. J., "Enhancement of Head-Disk Interface Durability by Use of Diamond-Like Carbon Overcoats on Slider's Rail," *IEEE Transactions on Magnetics*, Vol. 30, No. 2, pp. 369-374.

[55] Varanasi, S. S., Lauer, J. L., Talke, F. E., Wang, G., and Judy, J. H., "Friction and Wear Studies of Carbon Overcoated Thin Films Magnetic Sliders: Application of Raman Microspectroscopy," *Journal of Tribology – Transactions of the ASME*, Vol. 119, No. 3, July 1997, pp. 471-475.

[56] Bhatia, C. S., Anders, S., Brown, I. G., Bobb, K., Hsiao, R., and Bogy, D.B., "Ultra-thin Overcoats for the Head/Disk Interface Tribology," *Journal of Tribology – Transactions of the ASME*, Vol. 120, No. 4, October 1998, pp. 795-799.

[57] Kasai, P. H., Tang, W. T., and Wheeler, P., "Degradation of Perfluoropolyethers Catalyzed by Aluminum Oxide," *Applied Surface Science*, Vol. 51, September 1991, pp. 201-211.

[58] Chen, C. Y., Fong, W., Bogy, D. B., Bhatia, C. S., "Lubricant Thickness Effect on Tribological Performance of ZDOL Lubricated Disks with HydrogenatedOvercoats," *Technical Report 99-007 (Blue Series)*, Computer Mechanics Laboratory, University of California, Berkeley, CA, April 1999.

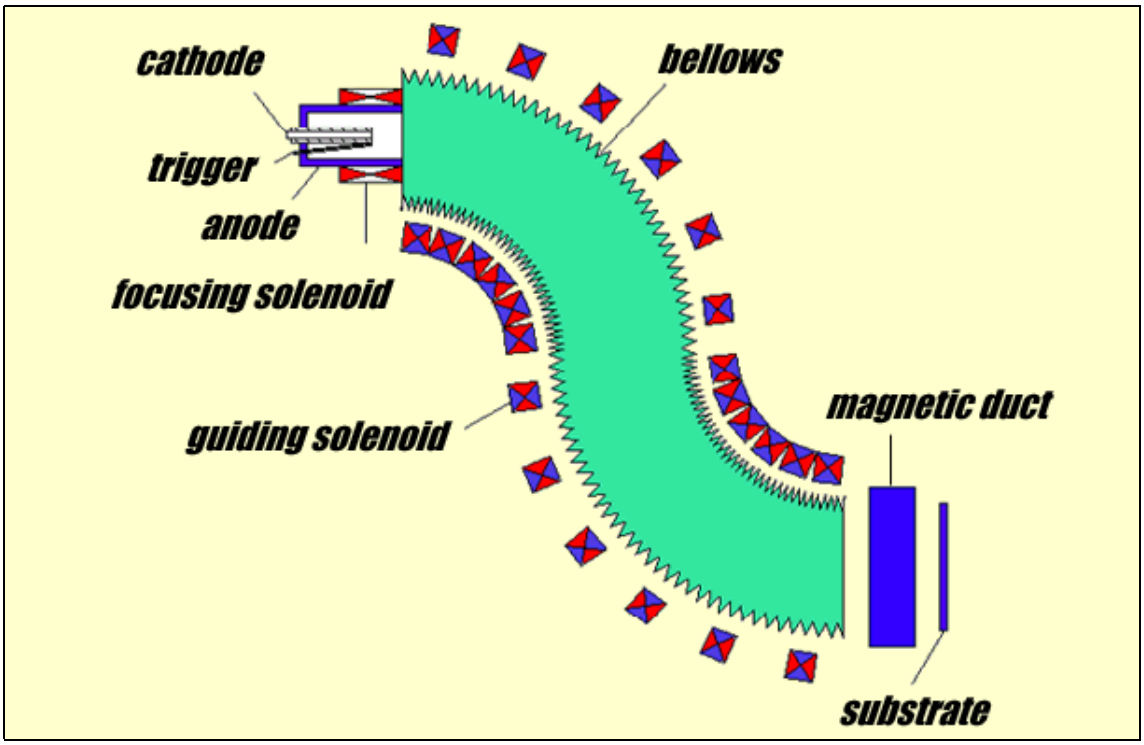

Figure 1. Schematic of cathodic-arc deposition method with solid-walled S-duct filter.

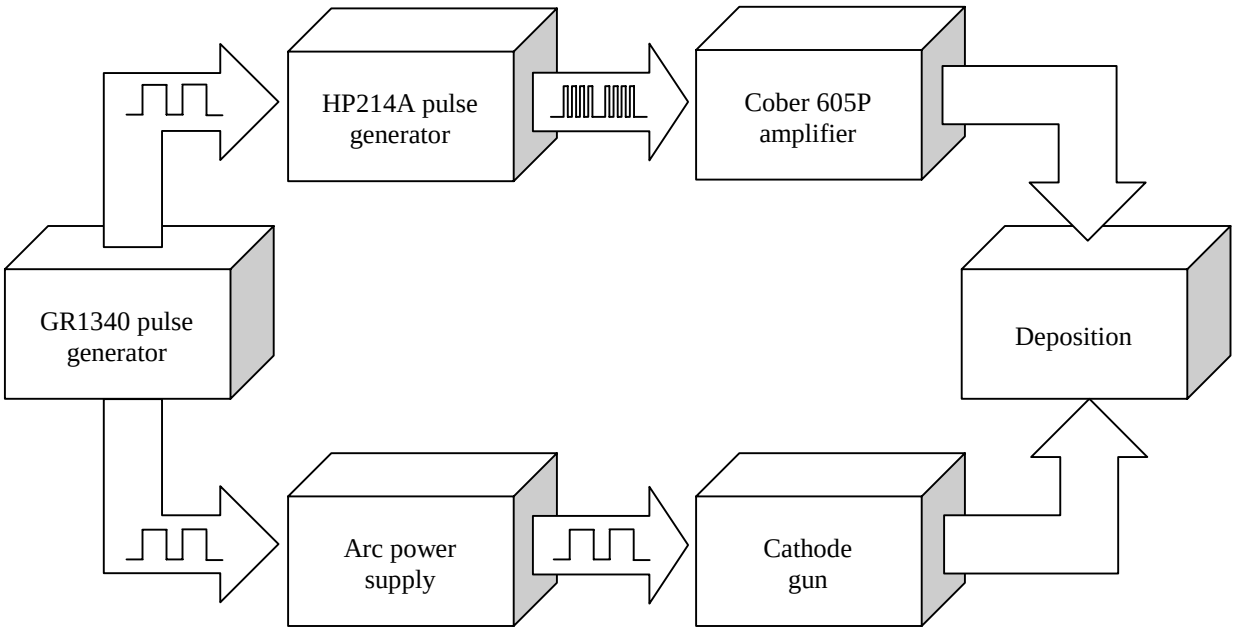

Figure 2. Cathodic-arc deposition flowchart.

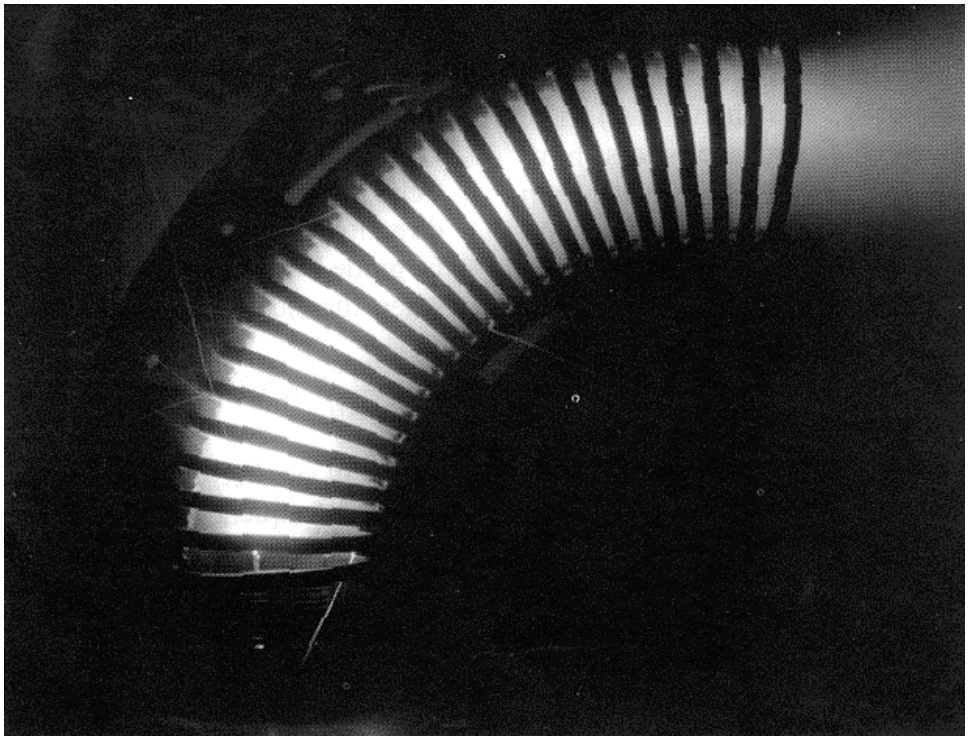

Figure 3. Open-walled 90° bent filter in operation [13].

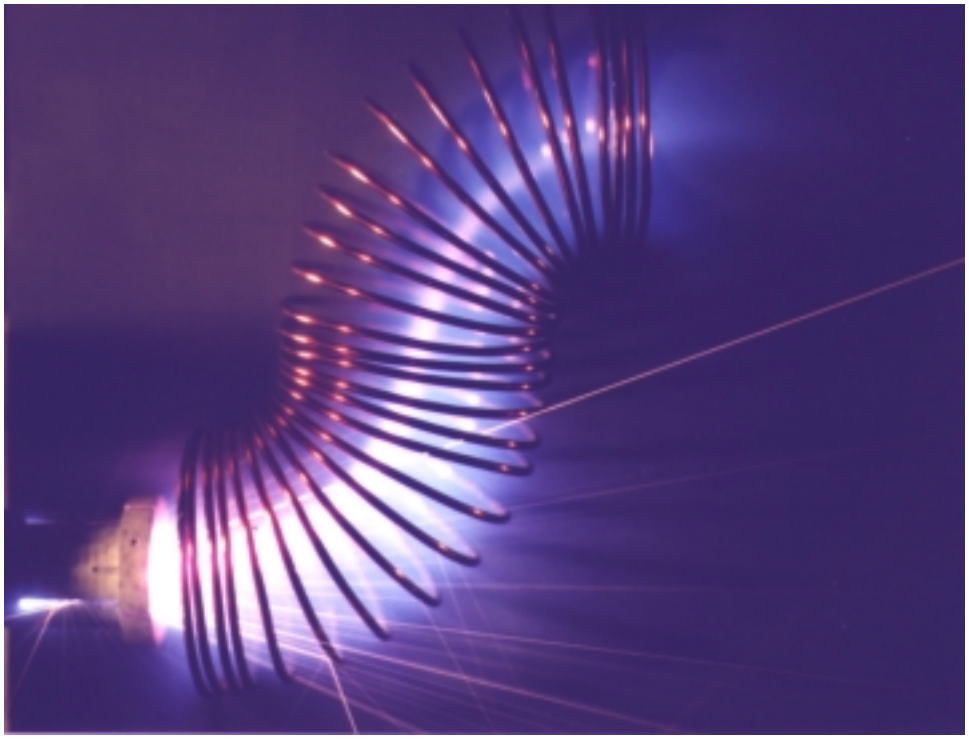

Figure 4. Open-walled S-duct filter in operation [33].

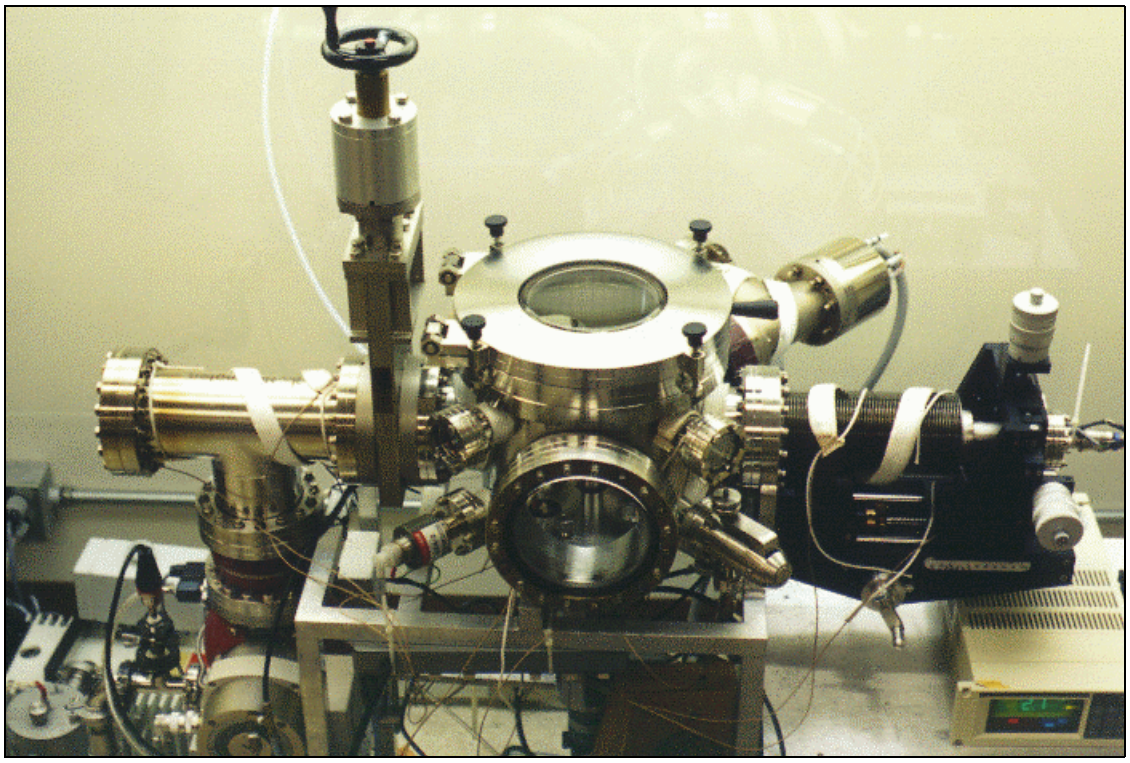

Figure 5. Ultra High Vacuum (UHV) tribochamber.

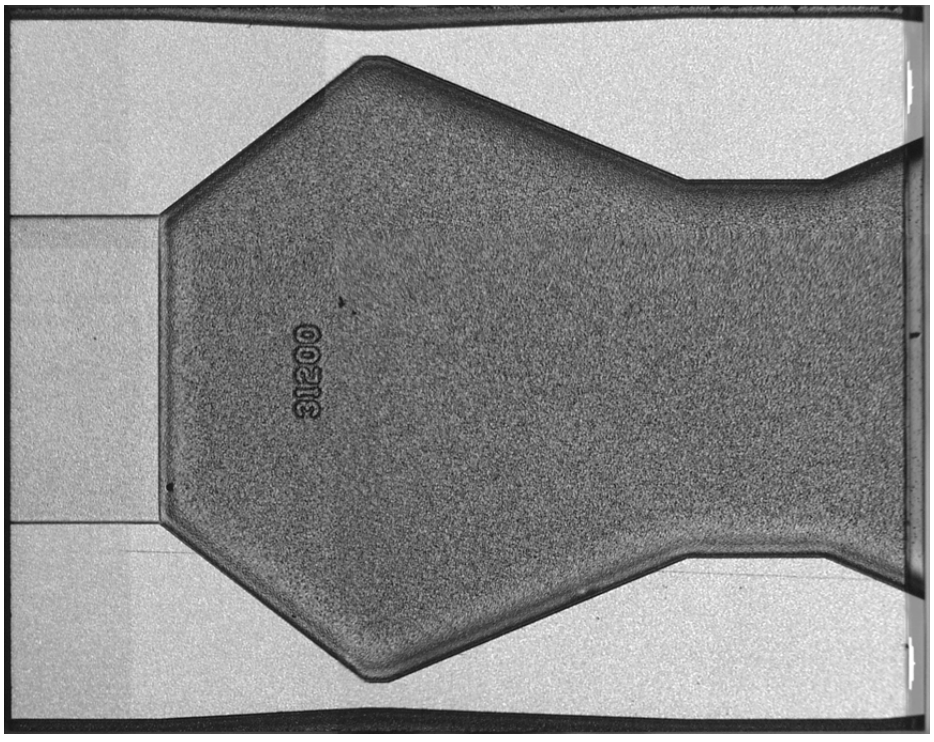

Figure 6. 50% slider air bearing surface.

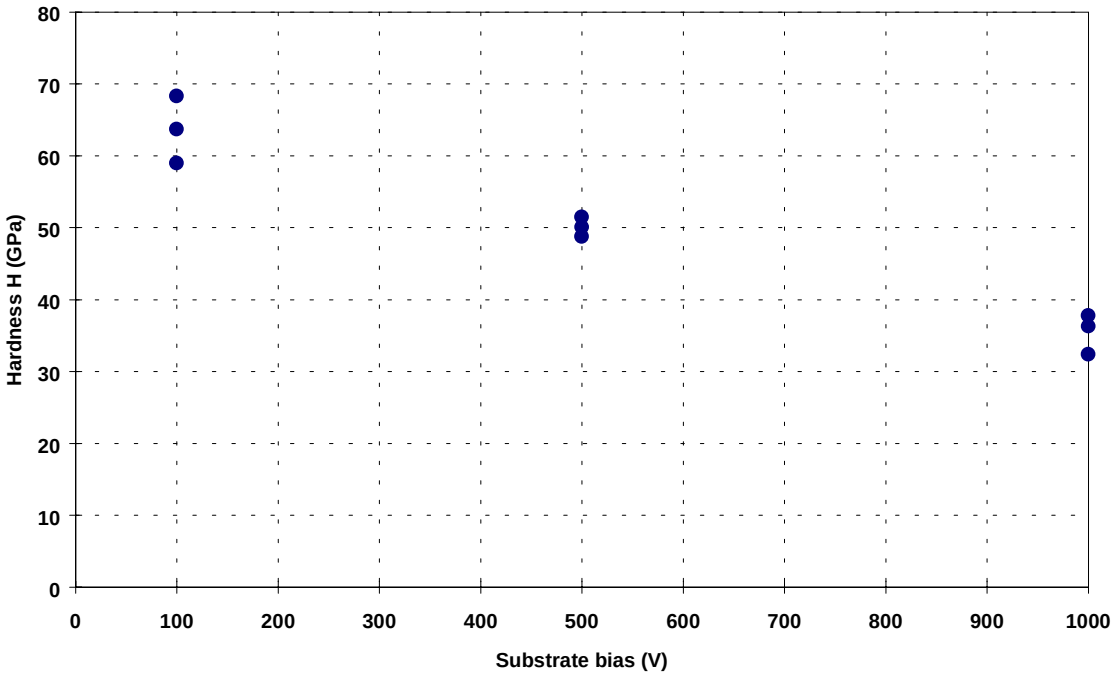

Figure 7. Plot of hardness H vs. substrate bias during deposition.

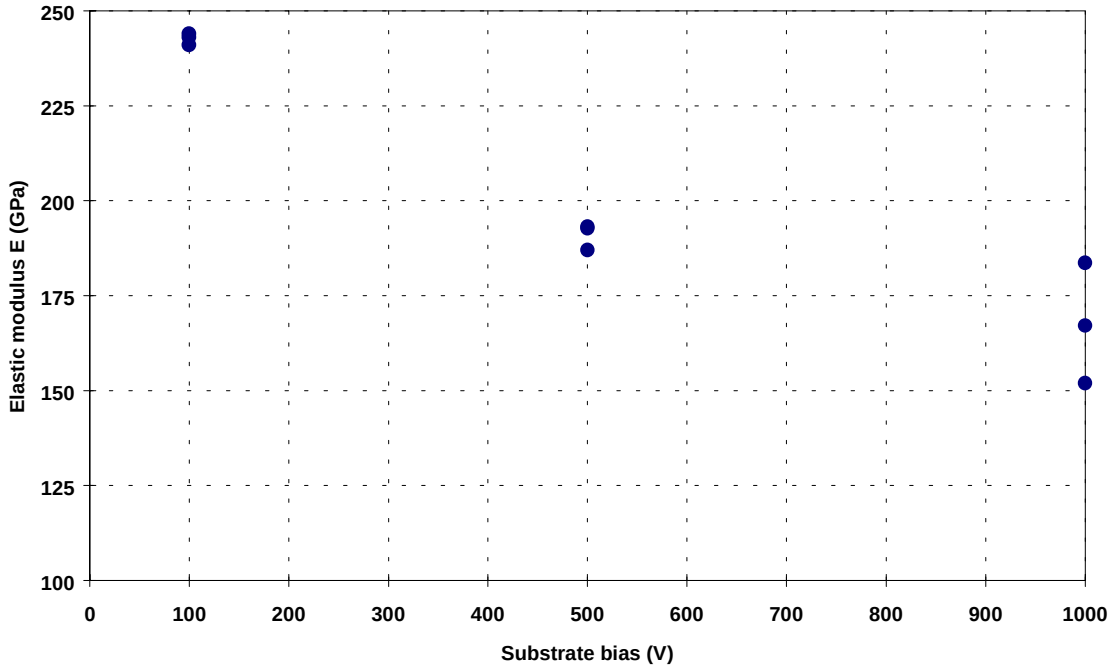

Figure 8. Plot of elastic modulus E vs. substrate bias during deposition.

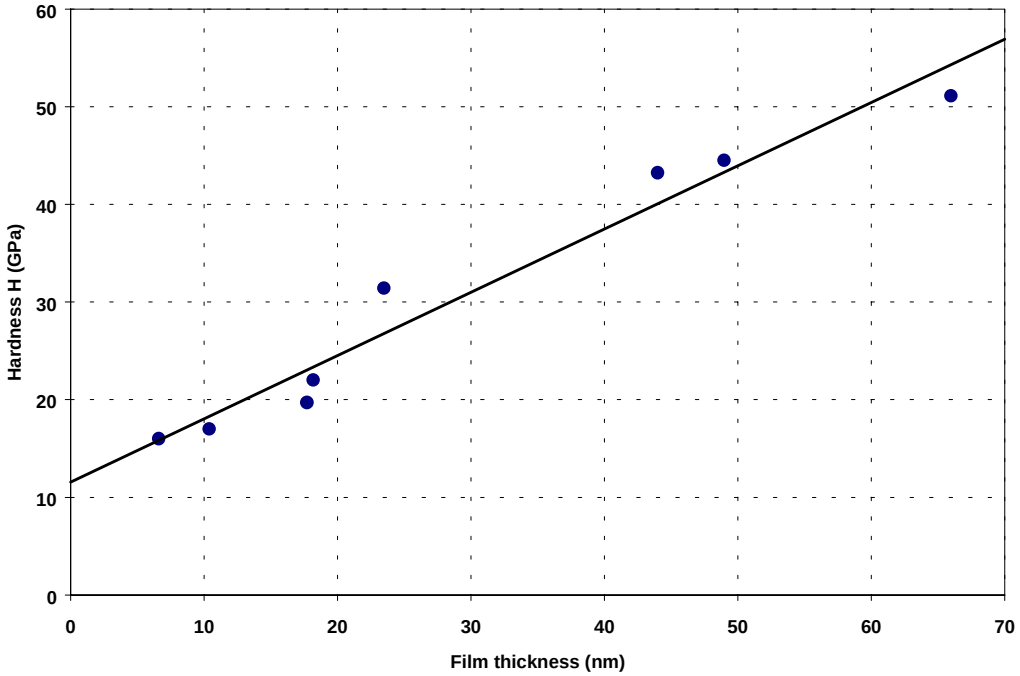

Figure 9. Plot of hardness H vs. film thickness.

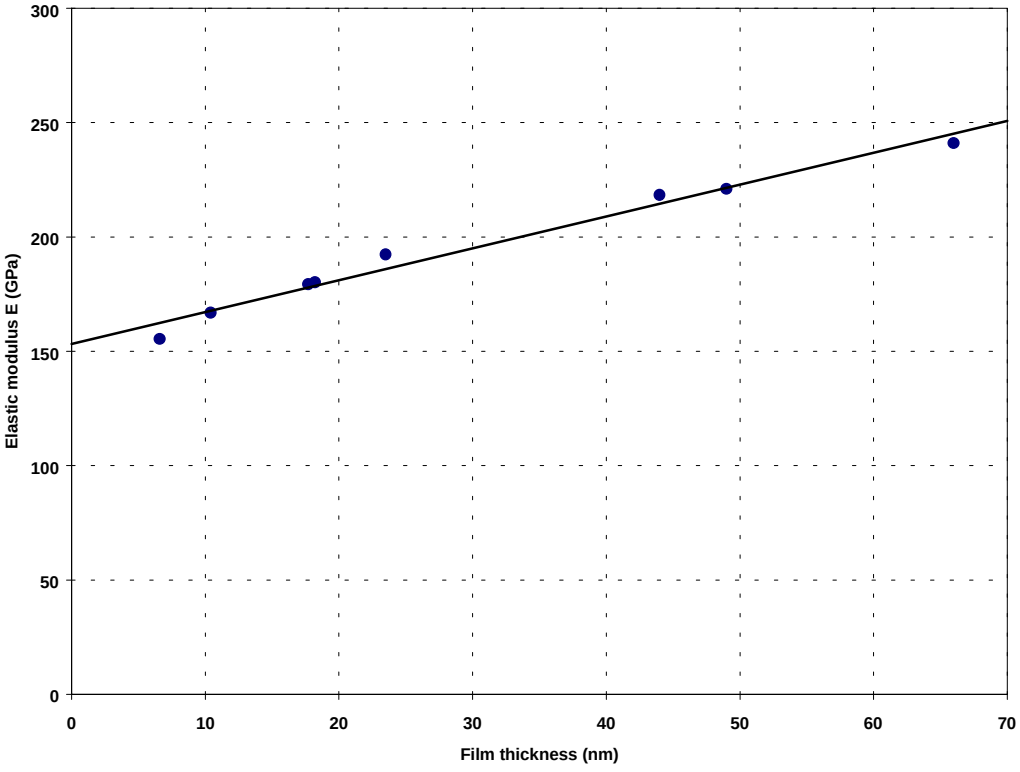

Figure 10. Plot of elastic modulus E vs. film thickness.

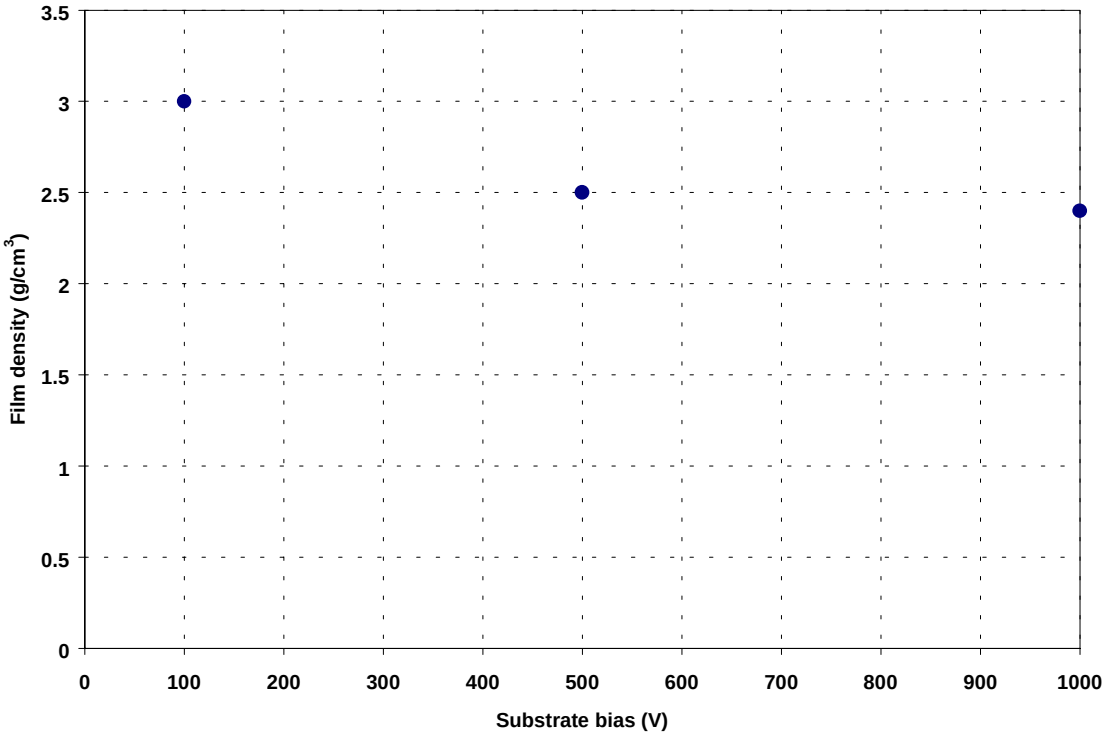

Figure 11. Film density vs. substrate bias during deposition.

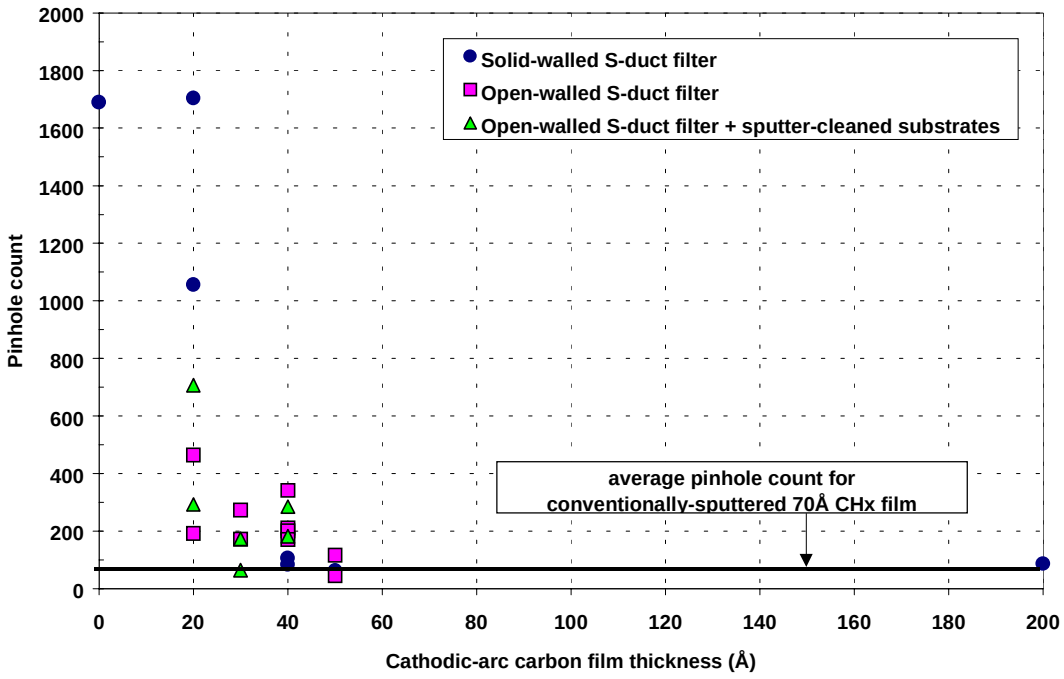

Figure 12. Corrosion pit count vs. film thickness.

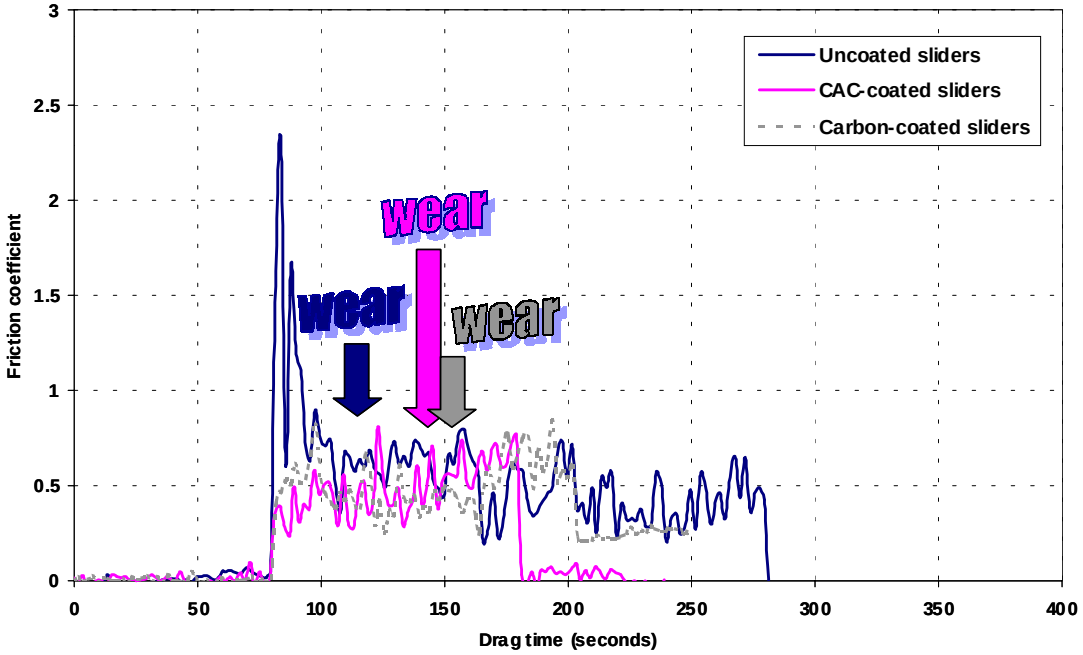

Figure 13. Friction coefficient vs. drag time for 50Å CAC disk lubricated with ZDOL.

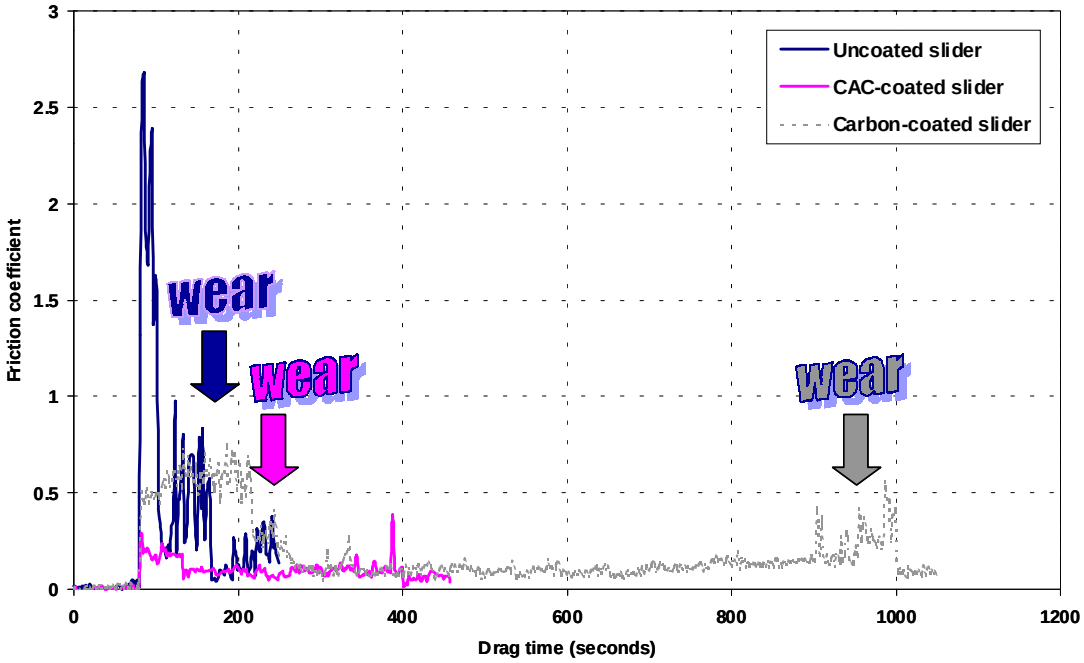

Figure 14. Friction coefficient vs. drag time for 50Å CH_x disk lubricated with ZDOL.

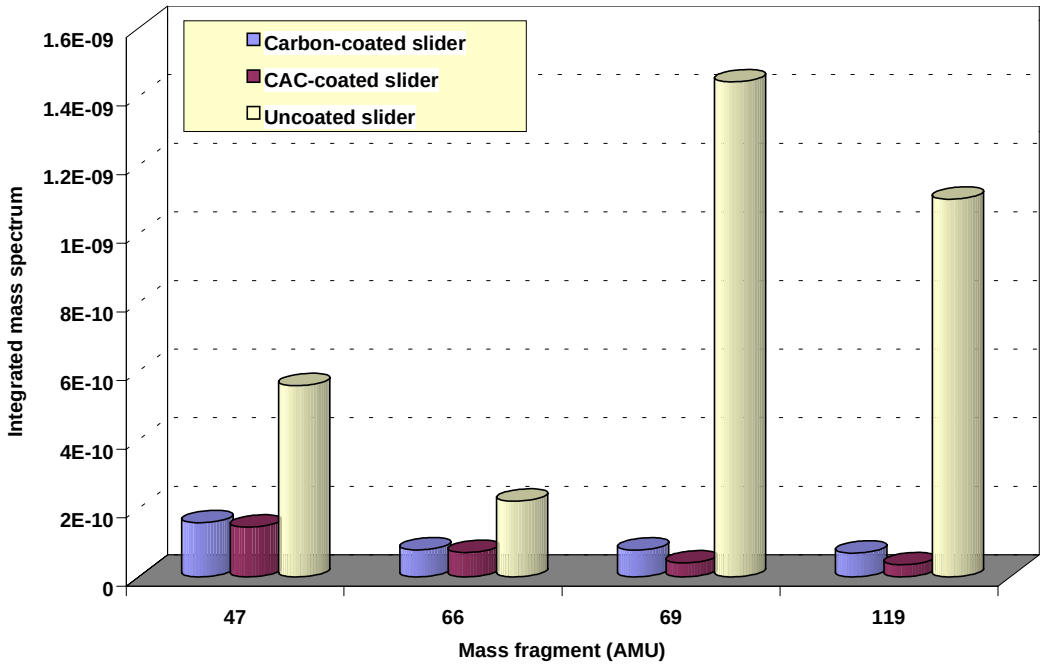

Figure 15. Integrated mass spectrum for drag tests with 50Å CH_x disk.

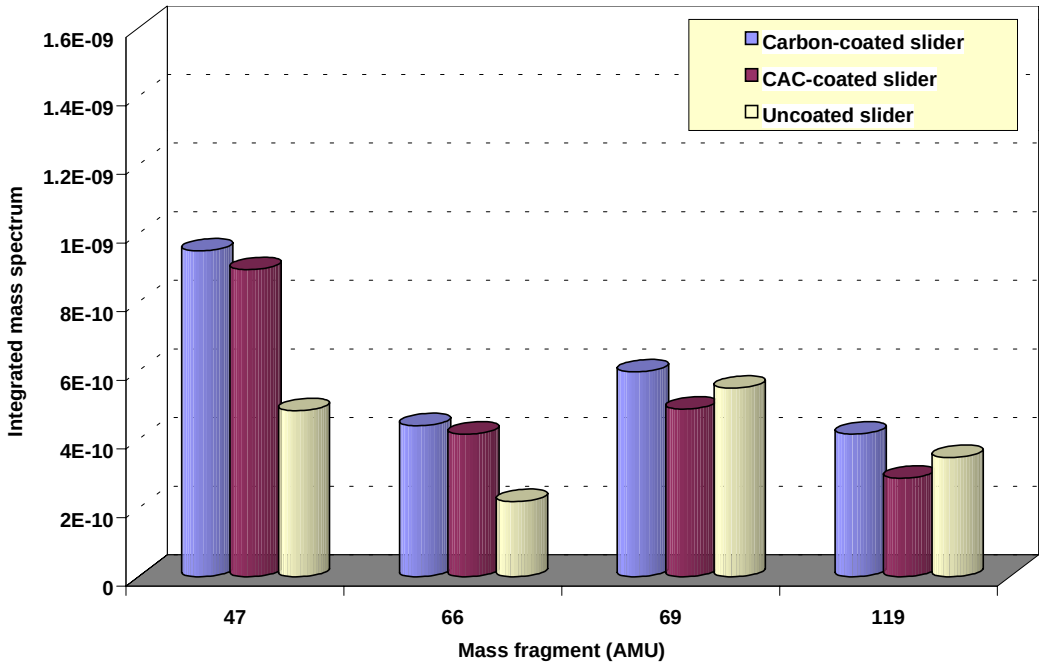

Figure 16. Integrated mass spectrum for drag tests with 50Å CAC disk.

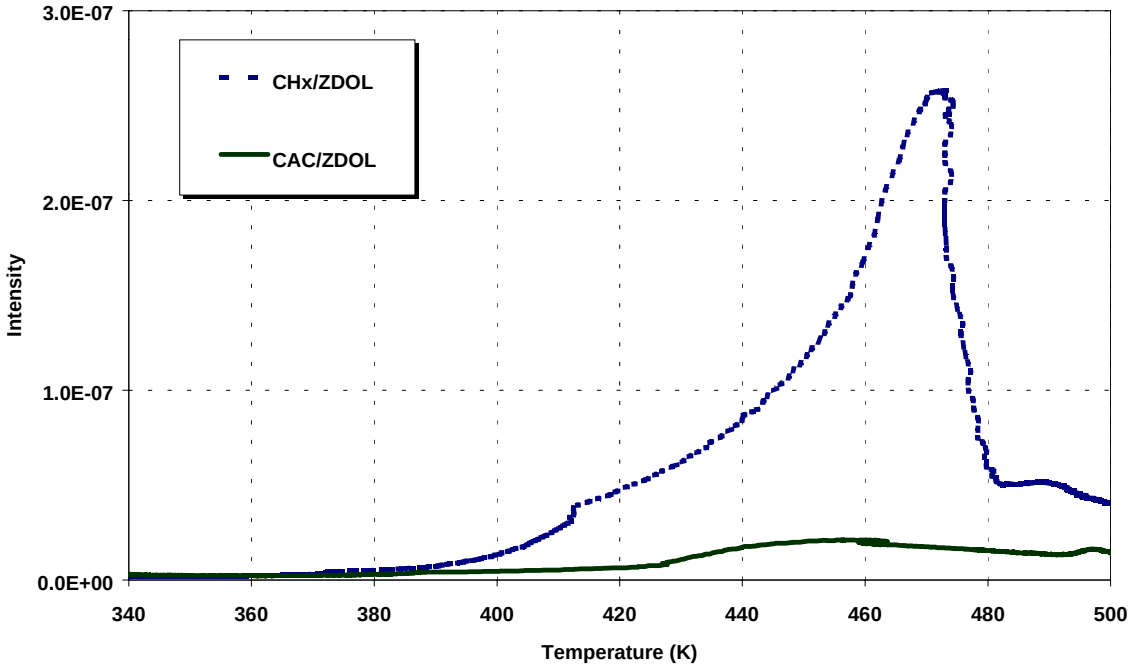

Figure 17. Thermal desorption profile for H_2.

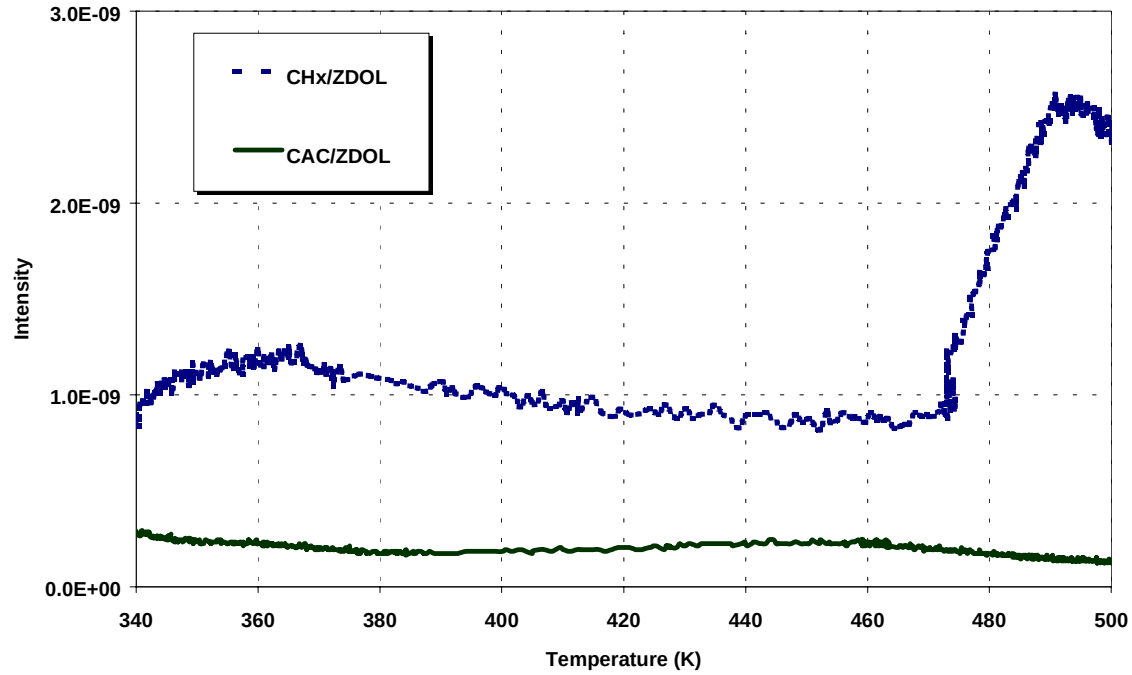

Figure 18. Thermal desorption profile for F.

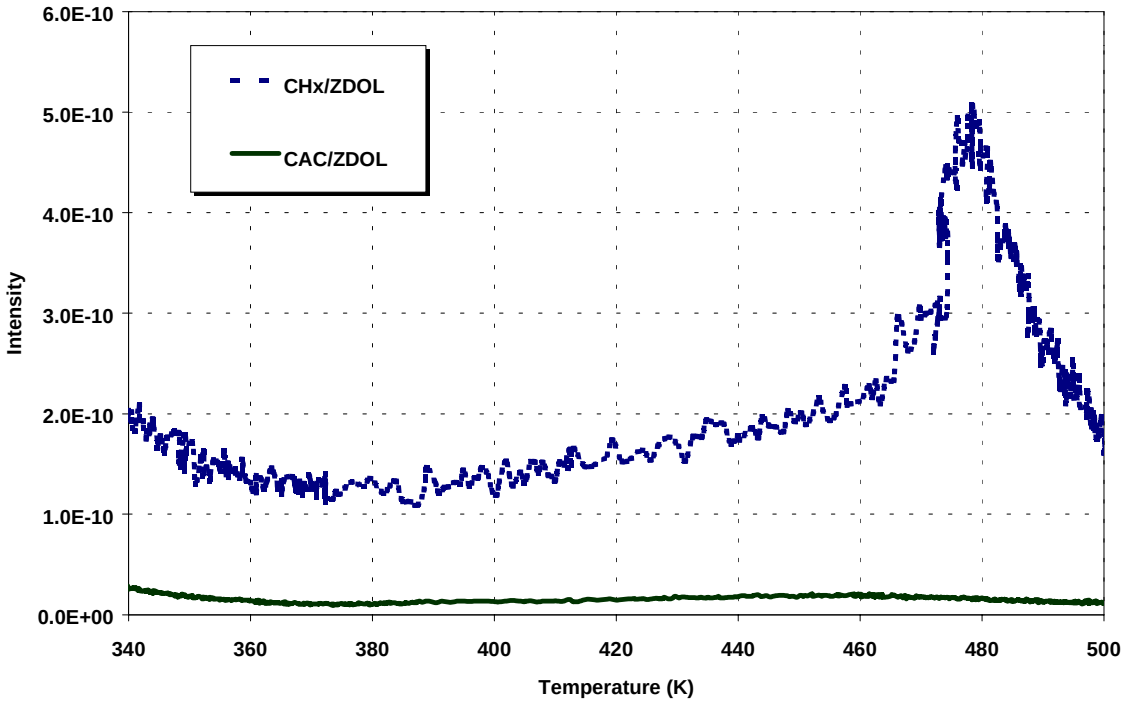

Figure 19. Thermal desorption profile for HF.